

Extended Near-Field Modelling and Droplet Size Distribution for Fuel-Air Explosive Warhead

S.K. Singh and V.P. Singh

Centre for Aeronautical Systems Studies & Analyses, Bangalore – 560 075

ABSTRACT

A theoretical model is developed for the prediction of the mean-mass diameter of droplets produced by the fragmentation of liquid fuel sheet and film in a fuel-air explosive (FAE) device after the detonation of the central burster charge. This model does not contain arbitrarily assumed values for the instabilities as in presently available models. Also, a distribution model for the initial distribution of the droplet diameter, which depends on the design parameters of the FAE device, is presented.

Keywords: Fuel-air explosive warhead, mean-mass diameter, dispersal modelling, fuel ejection mode

1. INTRODUCTION

The fuel-air explosive (FAE) is a relatively new warhead system which has been recognised as possessing much higher damage potential than the conventional TNT-based warheads for soft targets spread over large areas. In some quarters (especially in erstwhile USSR) it has been designated as a weapon of mass destruction. It may well be one of the more widely used future weapon systems.

The FAE mechanism is not new and is often encountered in everyday life. The combustion in the cylinder of an auto-engine is an FAE event and so is the explosion of coal dust in a mine. Historically, its use as a warhead goes back to world war II, when the Germans used a form of FAE against the Russians in the siege of Sebastopol. Initially, they used arrays of 28 cm and 32 cm barrage rockets to disperse fuels like gasoline, kerosene and naphtha, followed by 28 cm high

explosive rockets to detonate the fuel-air. The Soviets noted widespread personnel casualties due to blast¹.

Though the functioning of an FAE device does not involve very advanced physics, several phases of its functioning are still not well understood. In particular, the formation of the fuel-air cloud by the breaking of liquid fuel mass into droplets and the subsequent formation of a detonable fuel-air mixture is one such area. Attempts have been made to model the functioning^{1,2} of FAE, but a number of grey areas still exist. One of the most prominent trouble spots is a reliable estimation of the droplet size.

In this paper, a theoretical model for the estimation of mean-mass diameter (MMD) of the droplets rather than that of a single droplet has been presented. Also, a model for an initial distribution of the droplet diameter based on log normal distribution³ is presented.

2. FUEL-AIR EXPLOSIVE DEVICE

A typical FAE device consists of two coaxial metallic cylinders. The inner cylinder with much smaller radius compared to the outer one contains a burster charge of low velocity of detonation. The outer cylinder (also called the canister) is provided with longitudinal serrations to facilitate its opening in a petal-like manner⁴. A liquid fuel is placed in the space between the two cylinders. After the detonation of the central burster charge, a strong shock wave propagates through the liquid fuel. The canister is broken when the shock wave impinges upon it after propagating through the fuel. The liquid fuel is propelled outwards, first as liquid sheets through the cracked serrations and later as a coherent liquid shell when the canister is totally fragmented. The liquid shell moves outwards radially, with its thickness decreasing continuously till it is reduced to a very thin liquid film which ultimately breaks into a field of droplets. These droplets continue to move outwards, but due to their size (which is of the order of microns) the air drag comes into play and they stop after travelling some distance. The turbulent mixing of the droplets and the air produces a fuel-air cloud. When detonated after a pre-fixed delay, it gives rise to a strong blast wave which though of a relatively low peak overpressure has a much longer time duration (hence higher impulse) and much less spatial attenuation than TNT warheads. This fact makes it an effective weapon system against soft targets spread over large areas, such as troop concentration, mines, parked aircraft, etc.

The formation of a fuel-air cloud following the detonation of the central burster charge involves many complex processes. The dispersal process has been divided into three main regimes: (i) Ejection regime, in which the explosive forces of the burster charge predominate and accelerate the fuel mass, (ii) transition regime, in which the explosive forces are comparable to the fuel-air interaction forces which tend to decelerate the fuel mass, and (iii) expansion regime, in which the aerodynamic forces dominate the explosive forces, the fuel concentration in the cloud becomes low and the

shock waves decay into insignificance. The first two regimes together are termed as the near-field regime, whereas the third one is termed as far-field regime^{2, 5}.

3. EXTENDED NEAR-FIELD MODELLING

The initiation of the central burster charge takes place at one end and the detonation wave proceeds along its length. A strong shock wave propagates successively through the inner cylinder and the liquid fuel. This shock wave, on reaching the fuel-canister interface, generates extremely large stresses, which cause the canister to open longitudinally into a number of strips. A detailed mathematical model for the propagation of shock wave through various material media in an FAE device is available. There are two distinctly recognisable modes of fuel ejection when the canister opens up. These are (i) sheet mode, and (ii) shell mode.

3.1 Sheet Mode

This mode is applicable when the serrations are opening up but canister has not yet fully disintegrated. This mode lasts for a very small time. However, a significant mass of the liquid fuel is ejected from the longitudinal cracks along the serrations. The liquid rushes out in a nearly sheet form. As the sheet travels into air, instabilities are generated on its surface, which grow with time and lead to the disintegration of the sheet into ligaments, which subsequently break into droplets.

3.2 Shell Mode

Once the cracks propagating along the longitudinal serrations reach the other end of the canister, it is almost entirely fragmented and the leftover liquid is liberated as a radially expanding mass. Due to high initial velocity, this liquid mass continues to move radially outwards. Its thickness decreases continuously as it expands until it is reduced to a thin film. Due to the liquid film-air interaction, instabilities or perturbations grow on the film surface, which ultimately lead to its disintegration into droplets.

4. DISPERSION RELATIONS

4.1 Sheet Disintegration

The sheet disintegration has been extensively studied during the last half century. The first formulation for the disintegration of a viscous sheet was given by Dombrowsky and Johns⁶. As pointed out by Li and Tankin⁷, this formulation is valid only for large gas Weber number. Li and Tankin and Mitra and Li⁸ have presented a more systematic theory for the growth of instabilities, leading to its disintegration into droplets. However, since they assumed only Rayleigh mode of breakup for the ligaments into droplets, their theory resulted into much bigger droplet sizes. Lin and Kang⁹ pointed out that at higher sheet velocities, an atomisation mode of disintegration also exists for the jets and ligaments which gives much smaller droplets as observed in many physical situations. Since in a typical FAE device, the velocity of the liquid fuel sheets issuing from the cracks along the pre-formed serrations is quite high, it is appropriate to use the atomisation mode of ligament disintegration. It is also worth noting that Rayleigh mode is included as a sub-case in the atomisation mode.

Li and Tankin's formulation has been briefly presented for the growth of instabilities in a plane sheet along with atomisation mode of ligament disintegration due to Lin and Kang. Though in an FAE device, the width of the crack, and hence the thickness of the liquid sheet changes with time, in the proposed model, thickness of the liquid sheet was taken to be approximately constant. This simplifying assumption would be valid during the initial opening of the canister. In any case when the crack widens substantially, a switchover was made to the shell mode.

The motion of a 2-D liquid sheet was considered with density ρ_l , viscosity μ_l , surface tension σ and thickness $2a$, moving with a velocity U_0 through air which was assumed to be an inviscid fluid of density ρ_g . The sheet was moving in the radial direction, denoted by r . The direction along the crack width was denoted by y , with origin at the mid-plane of the sheet. Let a small perturbation in the sheet surface be given by

$$\xi = \xi_0 \exp(\omega t + ikr) \quad (1)$$

Then the two interfaces are given by $y = \pm a + \xi$, where $y = \pm a$ is the equilibrium position of the interfaces, ξ_0 is the initial amplitude of the disturbance ($\xi_0/a \ll 1$), k is the wave number of the disturbance which is related to the wavelength (λ) by the relationship $k = 2\pi/\lambda$; $\omega = \omega_r + i\omega_i$ is a complex variable. The real part of ω , ω_r represents the growth of the disturbance, whereas its imaginary part ω_i is 2π times the disturbance frequency.

The basic flow of the liquid sheet is a uniform flow of velocity U_0 along the r -direction with zero velocity along the y -direction. Let u , v be the perturbed velocity components of the liquid sheet in the r and y -directions, respectively and p be the pressure due to the disturbance. The quantities u , v and p are presumed to be very small. The linearised Navier-Stokes equations governing the perturbed motion are:

$$\frac{\partial u}{\partial r} + \frac{\partial v}{\partial y} = 0 \quad (2)$$

$$\frac{\partial u}{\partial t} + U_0 \frac{\partial u}{\partial r} = -\frac{1}{\rho_l} \frac{\partial p}{\partial r} + \nu_l \nabla^2 u \quad (3)$$

$$\frac{\partial v}{\partial t} + U_0 \frac{\partial v}{\partial r} = -\frac{1}{\rho_l} \frac{\partial p}{\partial y} + \nu_l \nabla^2 v \quad (4)$$

where $\nabla^2 = \partial^2/\partial r^2 + \partial^2/\partial y^2$ and ν_l is the kinematic viscosity of the liquid fuel.

Equations (2) to (4) are subjected to the following boundary conditions: At the interfaces $y \approx \pm a$, there is no net mass flux across the interfaces; the shear stress vanishes at the interface and the normal stress across the interface is continuous:

$$v = \frac{\partial \xi}{\partial t} + U_0 \frac{\partial \xi}{\partial r} \quad (5)$$

$$\tau_{ry} = \mu_l \left(\frac{\partial u}{\partial y} + \frac{\partial v}{\partial r} \right) = 0, \quad \tau_{yy} - \tau_{g,yy} = p_\sigma \quad (6)$$

where τ_{ry} and τ_{yy} are the liquid shear and normal stresses, respectively and $\tau_{g,yy}$ is the normal stress in air. To solve Eqns (2) to (4), Li and Tankin

suggested separation of the liquid velocity into inviscid and viscous parts as

$$u = u_1 + u_2, \quad v = v_1 + v_2 \quad (7)$$

where u_1, v_1 are the inviscid irrotational solutions in the liquid, and the leftover part u_2, v_2 contains the effect of liquid viscosity. For inviscid irrotational liquid flow, there exists a velocity potential (ϕ), such that $u_1 = \partial\phi / \partial r$, $v_1 = \partial\phi / \partial y$, and ϕ satisfies:

$$\nabla^2 \phi = 0 \quad (8)$$

The pressure is obtained by integrating the inviscid part of Eqn (3) wrt r as

$$p = -\rho_l \left(\frac{\partial\phi}{\partial t} + U_0 \frac{\partial\phi}{\partial r} \right) \quad (9)$$

The equations for the viscous parts reduce to

$$\frac{\partial u_2}{\partial r} + \frac{\partial v_2}{\partial y} = 0 \quad (10)$$

$$\left. \begin{aligned} \frac{\partial u_2}{\partial t} + U_0 \frac{\partial u_2}{\partial r} &= \nu_l \nabla^2 u_2 \\ \frac{\partial v_2}{\partial t} + U_0 \frac{\partial v_2}{\partial r} &= \nu_l \nabla^2 v_2 \end{aligned} \right\} \quad (11)$$

Next, Li and Tankin introduced a stream function like variable ψ , defined as $u_2 = \partial\psi / \partial y$, $v_2 = -\partial\psi / \partial r$.

From Eqn (11), one gets:

$$\frac{\partial\psi}{\partial t} + U_0 \frac{\partial\psi}{\partial r} = \nu_l \nabla^2 \psi \quad (12)$$

Considering the disturbances given in Eqn (1), ϕ and ψ are assumed to be of the following form:

$$\left. \begin{aligned} \phi &= \Phi(y) \exp(\omega t + ikr) \\ \psi &= \Psi(y) \exp(\omega t + ikr) \end{aligned} \right\} \quad (13)$$

Substituting Eqn (13) into Eqn (8) and Eqn (12) respectively, one gets:

$$\left. \begin{aligned} \Phi''(y) - k^2 \Phi(y) &= 0 \\ \Psi''(y) - s^2 \Psi(y) &= 0 \end{aligned} \right\} \quad (14)$$

where

$$s^2 = k^2 + (\omega + ikU_0) / \nu_l$$

Solving Eqn (14), one gets:

$$\left. \begin{aligned} \Phi &= (C_1 e^{ky} + C_2 e^{-ky}) \\ \Psi &= (C_3 e^{sy} + C_4 e^{-sy}) \end{aligned} \right\} \quad (15)$$

From the boundary conditions [Eqns (5) and (6)], the unknown constants are obtained as

$$\left. \begin{aligned} C_1 &= -C_2 = \frac{k^2 + s^2}{2k \cosh(ka)} \nu_l \xi_0 \\ C_3 &= C_4 = -\frac{ik}{\cosh(sa)} \nu_l \xi_0 \end{aligned} \right\} \quad (16)$$

Hence, the normal stress in the liquid fuel obtained as

$$\begin{aligned} \tau_{yy} &= -p + 2\mu_l \frac{\partial v}{\partial y} \\ &= [\{ \rho_l (\omega + ikU_0) + 2\mu_l k^2 \} (e^{ky} - e^{-ky}) C_1 \\ &\quad - 2i\mu_l ks (e^{sy} - e^{-sy}) C_3 \exp(\omega t + ikr)] \quad (17) \end{aligned}$$

The motion of the air, assumed as an inviscid and incompressible gas, is given by the following equations:

$$\frac{\partial u_g}{\partial r} + \frac{\partial v_g}{\partial y} = 0 \quad (18)$$

$$\left. \begin{aligned} \frac{\partial u_g}{\partial t} &= -\frac{1}{\rho_g} \frac{\partial p_g}{\partial r} \\ \frac{\partial v_g}{\partial t} &= -\frac{1}{\rho_g} \frac{\partial p_g}{\partial y} \end{aligned} \right\} \quad (19)$$

where the subscript g denotes the quantities for the gas medium. The boundary conditions require that across the liquid-gas interface the normal velocity be continuous, and far away from the liquid sheet the effects of the disturbances die out.

$$v_g = \frac{d\xi}{dt} \quad \text{at } y = |\pm a + \xi| \quad (20)$$

$$v_g = 0 \quad \text{as } |y| \rightarrow \infty \quad (21)$$

For the inviscid gas, the velocity can be expressed in terms of a velocity potential, which in accordance with Eqn (1) is assumed to be of the following form:

$$\phi_g = \Phi_g(y) \exp(\omega t + ikr) \quad (22)$$

Using the boundary conditions [Eqns (20) and (21)], the velocity potential is given by

$$\phi_s = -\frac{\omega}{k} \exp[k(a-|y|)] \xi_0 \exp(\omega t + ikr) \quad \text{for } |y| \geq a \quad (23)$$

Hence, the normal stress in the gas medium is given by

$$\begin{aligned} \tau_{s,yy} &= -p_s = \rho_s \frac{\partial \phi_s}{\partial t} \\ &= -\rho_s \frac{\omega^2}{k} \exp[k(a-|y|)] \xi_0 \exp(\omega t + ikr) \end{aligned} \quad (24)$$

4.1.1 Pressure Induced by Surface Tension

The pressure induced by the surface tension is given by

$$p_\sigma = \frac{\sigma}{R} \approx \sigma \frac{\partial^2 \xi}{\partial r^2} \quad (25)$$

where R is the radius of curvature of the interface. Using Eqn (1), p_σ is given by

$$p_\sigma = -\sigma k^2 \xi_0 \exp(\omega t + ikr) \quad (26)$$

The boundary condition [Eqn (6)] (viz., the continuity of normal stresses across the interface), on substitution from Eqns (17), (24) and (26) at $y = a$ gives the following relationship between the complex growth rate (ω) and the disturbance wave number (k) (the dispersion relation) as

$$\begin{aligned} [\rho_l(\omega + ikU_0) + 2\mu_l k^2][\nu_l(k^2 + s^2)] \tanh(ka) \\ - 4\mu_l \nu_l k^3 \operatorname{stnh}(sa) + \rho_g \omega^2 + \sigma k^3 = 0 \end{aligned} \quad (27)$$

By putting $\mu_l = 0$ in Eqn (27), the inviscid dispersion relationship was obtained.

4.2 Cylindrical Liquid Film Disintegration

Unlike the liquid film disintegration, not much literature is available for the disintegration of a cylindrical liquid film. Gardner² proposed an analytical model for the growth of instabilities in the liquid film, leading to its breakup into droplets and also attempted to estimate the diameter of a single drop. Though the physical phenomenon was reasonably modelled, the initial values for instabilities were chosen rather arbitrarily which

introduced uncertainties in the estimation of the droplet size.

In this paper, an attempt has been made to incorporate the concept of dispersion relation by an alternative formulation for the growth of instabilities in the cylindrical film which enables one to get rid of arbitrary assumed initial values for the instabilities. Further, it also enables one to establish a relationship with the well-studied sheet case. Li and Tankin⁷ and Mitra and Li⁸, *et al* introduced the viscosity via a specially defined stream function approach. Since stream functions are not available for a truly 3-D flow, the study was restricted presently to inviscid case only. Based on a comparison of results in the plane sheet case, it was found that the maximum error in the droplet size does not exceed 10 per cent when the viscous formulation was replaced by an inviscid one.

A cylinder of fluid, denoted fluid 1, of radius $r_l(t)$ and of height z_s was considered. This was surrounded by an annulus of fluid, denoted as fluid 2, of outer radius $r_o(t)$ and also of height z_s . Surrounding this annulus of fluid 2 was an infinite fluid medium, denoted as fluid 3. The interface between the fluids 1 and 2 was denoted interface 1, and that between the fluids 2 and 3, interface 2. With reference to an FAE device, fluid 1 represented the detonation product gases produced by the detonation of the burster charge. Fluid 2 represented the liquid fuel to be dispersed and fluid 3 represented the ambient atmosphere. Thus, the liquid shell consisting of fluid 2 expands radially after the detonation of burster charge till this shell was reduced to a very thin liquid film. Instabilities in waveform propagated in the liquid film whose amplitude grew till it was broken into ligaments, which were subsequently broken into droplets.

Using the usual cylindrical coordinate system (r, θ, z), the basic radial motion of the liquid shell perturbs by the small amount as

$$\begin{aligned} r_1 &= r_l + \xi_1 \exp[\omega t + i(kz + n\theta)] \\ r_2 &= r_o + \xi_2 \exp[\omega t + i(kz + n\theta)] \end{aligned} \quad (28)$$

where k is the axial wave number, n is an integer and as in the plane sheet case, $\omega = \omega_r + i\omega_i$ is a complex variable with its real part ω_r , as the rate of

growth of the disturbance and the imaginary part ω_i as 2π times the frequency.

The situation was considered when the film had become very thin, i.e. when $r_0 - r_i$ was a small quantity and it was assumed that at this moment $\xi_1 = \xi_2 = \xi_0$ (say). The preceding motion was assumed to be governed by Gardner's model². The radial velocity $U_0 \approx \dot{r}_0$ is the basic velocity component and let v_r, v_θ and v_z be the perturbed velocity components along r, θ and z -directions, respectively. The linearised equations of motion for the inviscid fluid are:

$$\frac{\partial v_r}{\partial t} + U_0 \frac{\partial v_r}{\partial r} = -\frac{1}{\rho_l} \frac{\partial p}{\partial r} \tag{29}$$

$$\frac{\partial v_\theta}{\partial t} + U_0 \frac{\partial v_\theta}{\partial r} = -\frac{1}{\rho_l} \frac{1}{r} \frac{\partial p}{\partial \theta} \tag{30}$$

$$\frac{\partial v_z}{\partial t} + U_0 \frac{\partial v_z}{\partial r} = -\frac{1}{\rho_l} \frac{\partial p}{\partial z} \tag{31}$$

where ρ_l is the density of the liquid and p is the perturbation pressure. Since the flow is inviscid and irrotational, there exists a velocity potential ϕ , such that

$$v_r = \frac{\partial \phi}{\partial r}, \quad v_\theta = \frac{\partial \phi}{\partial \theta}, \quad v_z = \frac{\partial \phi}{\partial z} \tag{32}$$

and ϕ satisfies the following Laplace's equation:

$$\frac{\partial^2 \phi}{\partial r^2} + \frac{1}{r} \frac{\partial \phi}{\partial r} + \frac{1}{r^2} \frac{\partial^2 \phi}{\partial \theta^2} + \frac{\partial^2 \phi}{\partial z^2} = 0 \tag{33}$$

In view of the disturbances given by Eqn (28), ϕ may be assumed in the following form:

$$\phi = \Phi(r) \exp[\omega t + i(kz + n\theta)] \tag{34}$$

Using Eqn (34), Eqn (33) reduces to:

$$r^2 \Phi'' + r \Phi' - (n^2 + k^2 r^2) \Phi = 0 \tag{35}$$

which is modified Bessel's equation with general solution $\Phi = C_1 I_n(kr) + C_2 K_n(kr)$, where I_n and K_n are modified Bessel's functions of the first and the second kind, respectively. For the fluid 1, which includes the origin, $C_2 = 0$ (since $K_n(r) \rightarrow \infty$ as $r \rightarrow 0$). Also, for the unperturbed or the basic radial

motion, the velocity potential is $\phi_{1u} = r_i \dot{r}_i \log r$. The total velocity potential as the sum of unperturbed and perturbed parts is given by

$$\phi_1 = r_i \dot{r}_i \log r + \left\{ \frac{\xi_1 (\omega + \dot{r}_i / r_i)}{k I_n'(kr_i)} \right\} \times I_n(kr) \exp[\omega t + i(kz + n\theta)] \tag{36}$$

Similarly for the fluid 3 (i.e. the unbounded air), the velocity potential is given by

$$\phi_3 = r_0 \dot{r}_0 \log r + \left\{ \frac{\xi_2 (\omega + \dot{r}_0 / r_0)}{k K_n'(kr_0)} \right\} \times K_n(kr) \exp[\omega t + i(kz + n\theta)] \tag{37}$$

The velocity potential for the fluid 2 (i.e. the liquid fuel) is given by

$$\begin{aligned} \phi_2 = & \dot{r}_0 r_0 \log r \\ & + \left\{ \xi_1 (\omega + \dot{r}_i / r_i) \frac{[K_n'(kr_0) I_n(kr) - I_n'(kr_0) K_n(kr)]}{k [I_n'(kr_i) K_n'(kr_0) - I_n'(kr_0) K_n'(kr_i)]} \right\} \\ & + \xi_2 (\omega + \dot{r}_0 / r_0) \frac{[K_n'(kr_0) I_n(kr) - I_n'(kr_i) K_n(kr)]}{k [I_n'(kr_0) K_n'(kr_i) - I_n'(kr_i) K_n'(kr_0)]} \\ & \times \exp[\omega t + i(kz + n\theta)] \end{aligned} \tag{38}$$

Next, from Eqn (29), the pressure in fluid 2 is given by

$$p_2 = -\rho_l \left(\frac{\partial \phi_2}{\partial t} + U_0 \frac{\partial \phi_2}{\partial r} \right) \tag{39}$$

Using Eqn (38) for a thin film, Eqn (39) reduces to

$$\begin{aligned} p_2 = & -2\rho_l \left[\dot{r}_0^2 \left(1 - \frac{\xi_0}{r_0} \exp[\omega t + i(kz + n\theta)] \right) \right. \\ & \left. + \dot{r}_0 \xi_0 \left(\omega + \frac{\dot{r}_0}{r_0} \right) \exp[\omega t + i(kz + n\theta)] \right] \end{aligned} \tag{40}$$

Since the velocity is continuous at the liquid-gas interface, one has at $r = r_0, U_{gas} = U_{liqu} \approx \dot{r}_0$. The pressure is given by $p_3 = -\rho_g (\partial \phi_3 / \partial t)$.

Using Eqn (37), one gets:

$$\begin{aligned}
 p_3 = & -\rho_g \left[\dot{r}_0^2 \left(1 - \frac{\xi_0}{r_0} \exp[\omega t + i(kz + n\theta)] \right) \right. \\
 & + \left. \left\{ \dot{r}_0 \xi_0 \left(\omega + \frac{\dot{r}_0}{r_0} \right) + \frac{\omega \xi_0 K_n(kr_0)}{kK'_n(kr_0)} \right\} \right. \\
 & \left. \times \exp[\omega t + i(kz + n\theta)] \right] \quad (41)
 \end{aligned}$$

The radial stresses in the liquid and the gas medium are: $\tau_{l,rr} = -p_2$ and $\tau_{g,rr} = -p_3$, respectively. Since the normal or the radial stresses are continuous across the liquid-gas interface, one has:

$$\tau_{l,rr} - \tau_{g,rr} = p_\sigma = \frac{2\sigma}{R} \quad (42)$$

where σ is the surface tension and R is the radius of curvature which for the thin film is given by

$$\frac{1}{R} = \frac{1}{r_0} \left[1 - (n^2 + 1) \frac{\xi_0}{r_0} \exp[\omega t + i(kz + n\theta)] \right] \quad (43)$$

Using Eqns (40) and (41) in Eqn (42), one gets:

$$\begin{aligned}
 2\rho_l \left[\dot{r}_0^2 \left(1 - \frac{\xi_0}{r_0} \exp[\omega t + i(kz + n\theta)] \right) \right. \\
 + \left. \dot{r}_0 \xi_0 \left(\omega + \frac{\dot{r}_0}{r_0} \right) \exp[\omega t + i(kz + n\theta)] \right] \\
 - \rho_g \left[\dot{r}_0^2 \left(1 - \frac{\xi_0}{r_0} \exp[\omega t + i(kz + n\theta)] \right) + \left\{ \dot{r}_0 \xi_0 \left(\omega + \frac{\dot{r}_0}{r_0} \right) \right. \right. \\
 + \left. \left. \frac{\omega \xi_0 K_n(kr_0)}{kK'_n(kr_0)} \right\} \times \exp[\omega t + i(kz + n\theta)] \right] \\
 = \frac{2\sigma}{r_0} \left[1 - (n^2 + 1) \frac{\xi_0}{r_0} \exp[\omega t + i(kz + n\theta)] \right] \quad (44)
 \end{aligned}$$

To the zeroth-order of ξ_0 , one obtains the following expression from Eqn (44):

$$(2\rho_l - \rho_g) \dot{r}_0^2 = \frac{2\sigma}{r_0} \quad (45)$$

which is satisfied by the unperturbed radial motion of the liquid film. To the first-order of ξ_0 , one obtains the following expression from Eqn (44):

$$\begin{aligned}
 2\rho_l \left[-\frac{\dot{r}_0^2 \xi_0}{r_0} + \dot{r}_0 \xi_0 \left(\omega + \frac{\dot{r}_0}{r_0} \right) \right] - \rho_g \left[-\frac{\dot{r}_0^2 \xi_0}{r_0} \right. \\
 + \left. \dot{r}_0 \xi_0 \left(\omega + \frac{\dot{r}_0}{r_0} \right) + \frac{\omega \xi_0 K_n(kr_0)}{kK'_n(kr_0)} \right] = -\frac{2(n^2 + 1)\sigma \xi_0}{r_0} \quad (46)
 \end{aligned}$$

which is the dispersion relation for the cylindrical film.

5. ESTIMATION OF MEAN-MASS DIAMETER

5.1 Dispersion Relations

The dispersion relations [Eqn (27) or Eqn (46)] play a very important role in the disintegration process of a plane sheet or a thin cylindrical film, respectively as these provide information about the most dominant wave number, which is likely to get amplified, leading to the breakup of the sheet or the film.

5.1.1 Sheet Case

The wave number k for a typical FAE data is of the order of 10^5 or more, hence $\tanh(ka) \rightarrow 1$, $\tanh(sa) \rightarrow 1$, and Eqn (27) reduces to the following expression:

$$(2\nu_l k^2 + \omega + ikU_0)^2 - 4\nu_l^2 k^3 s + \tilde{\rho} \omega^2 + \frac{\sigma k^3}{\rho_l} = 0 \quad (47)$$

where only the real part of Eqn (47) was considered and using $\omega_i = (1 + \tilde{\rho})^{-1} (-kU_0 \pm ikm)$, (see Appendix), where $m^2 = \tilde{\rho}U_0^2 - \sigma k(1 + \tilde{\rho})/\rho_l$,

$\tilde{\rho} = \frac{\rho_g}{\rho_l}$, one gets after some simplifications:

$$\begin{aligned}
 4\nu_l^2 k^4 + (1 + \tilde{\rho}) \left(\omega_r \pm \frac{km}{1 + \tilde{\rho}} \right)^2 + 4\nu_l k^2 \left(\omega_r \pm \frac{km}{1 + \tilde{\rho}} \right) \\
 - \tilde{\rho}(1 + \tilde{\rho}) \left(\frac{kU_0}{1 + \tilde{\rho}} \right)^2 - 4\nu_l^2 k^3 r^{1/2} \\
 \times \frac{\cos(\gamma/2) \sinh(2ar^{1/2} \cos(\gamma/2))}{\cosh(2ar^{1/2} \cos(\gamma/2)) + \cos(2ar^{1/2} \sin(\gamma/2))} \\
 - \frac{\sin(\gamma/2) \sin(2ar^{1/2} \sin(\gamma/2))}{\cosh(2ar^{1/2} \cos(\gamma/2)) + \cos(2ar^{1/2} \sin(\gamma/2))} \\
 + \frac{\sigma k^3}{\rho_l} = 0 \quad (48)
 \end{aligned}$$

where

$r = (a^2 + b^2)^{1/2}$, $\gamma = \tan^{-1}(b/a)$ and $a = k^2 + v_i^{-1}(\omega_r \pm km/(1 + \tilde{\rho}))$, $b = v_i^{-1} \tilde{\rho} k U_o / (1 + \tilde{\rho})$.

For the inviscid case (i.e. $v_i = 0$), the Eqn (48) assumes a much simpler form in which ω_r can be explicitly expressed as

$$\omega_r = \frac{2}{1 + \tilde{\rho}} \left[U_o^2 \tilde{\rho} k^2 - \frac{1}{\rho_l} \sigma k^3 (1 + \tilde{\rho}) \right]^{1/2} \quad (49)$$

It is obvious from Eqn (49) that $\omega_r = 0$ only for $k = 0$ and $k = U_o^2 \tilde{\rho} / (\rho_l^{-1} \sigma / (1 + \tilde{\rho})) \equiv k_{lim}$ (say). The maximum value of ω_r is given by

$$\frac{d\omega_r}{dk} = 0 \quad (50)$$

which gives

$$k_{max} = \frac{2U_o^2 \tilde{\rho}}{3\rho_l^{-1} \sigma (1 + \tilde{\rho})} = \frac{2}{3} k_{lim} \quad (51)$$

The most unstable wave⁸ or the wave of maximum growth⁶ occurs at the maximum value of ω_r for both viscous and inviscid cases and is given by the relation [Eqn (50)], from which the corresponding wavelength λ_1 is obtained using the relation $\lambda_1 = 2\pi/k_{max}$. In the case of a plane sheet, waves grow on the sheet until they reach the critical amplitude. Tears occur in the crests and troughs and fragments of the sheet corresponding to one-half wavelength are broken off^{6,8}. The fragments contract by surface tension into unstable ligaments whose diameter, d_L is given by

$$\frac{1}{4} \pi d_L^2 = \lambda_1 a \quad (52)$$

5.1.2 Ligament Breaking Modes

The ligaments produced thus further break down into individual droplets. Mitra and Li⁸ used the classical axisymmetric breaking mode due to Rayleigh^{10,12} which resulted in much bigger droplet diameters. Lin and Kang on the other hand showed that Rayleigh breaking mode was valid only at lower speeds, whereas at higher speeds atomisation mode would occur, resulting in much smaller droplet diameters.

(a) Rayleigh's Axisymmetric Breaking Mode

The well-known result for a jet or a ligament predicts its breaking by amplification of wave type instabilities, whose wavelength is given by

$$\lambda_2 = 4.50 d_L \quad (53)$$

where d_L is the diameter of the jet or the ligament.

(b) Atomisation Mode

Lin and Kang have derived the dispersion relation in non-dimensional form as

$$\begin{aligned} & (\omega - ik)^2 + \frac{2k^2}{\text{Re}} \left(\frac{I_1'(k)}{I_0(k)} - \frac{2k\zeta}{\zeta^2 + k^2} \frac{I_1(k)I_1'(\zeta)}{I_0(k)I_1(\zeta)} \right) \\ & \times (\omega - ik) + \omega^2 \tilde{\rho} \frac{\zeta^2 - k^2}{\zeta^2 + k^2} \frac{K_0(k)I_1(k)}{K_1(k)I_0(k)} \\ & - \text{We}^{-1} k(1 - k^2) \times \frac{\zeta^2 - k^2}{\zeta^2 + k^2} \frac{I_1(k)}{I_0(k)} = 0 \end{aligned} \quad (54)$$

where $\zeta^2 = k^2 + \text{Re}(\omega - ik)$, Re being the Reynolds number $\equiv U_o d_L / (2\nu_i)$, $\text{We} = 2\sigma / \rho_l U_o^2 d_L$ is the Weber number. It is interesting to note that for the inviscid case and for $\tilde{\rho} \rightarrow 0$, Eqn (54) reduces to the Rayleigh's result for the breakup of low velocity ligament or jet. Further for $k \rightarrow \infty$, its dimensional form reduces to Eqn (47), which leads to $\lambda_2 = \lambda_1$.

5.2 Estimation of Mean-Mass Diameter

When the wavelength λ_2 of the instabilities developed on the ligament is known, the mean-mass diameter (MMD), D_{30} is estimated from the conservation of mass as

$$\frac{\pi}{4} d_L^2 \lambda_2 = \frac{\pi}{6} D_{30}^3 \quad (55)$$

5.2.1 Cylindrical Film Case

The dispersion relation for this case is given by Eqn (46). Considering only its real part as in the sheet case, the relation between ω_r and k is obtained as

$$\omega_r = \frac{km}{1 + \tilde{\rho}} - \frac{2(n^2 + 1)\sigma / \rho_l r_o^2}{(2 - \tilde{\rho}) \dot{r}_o - \tilde{\rho} K_n(kr_o) / kK_n'(kr_o)} \quad (56)$$

where

$$m = [\tilde{\rho} \dot{r}_0^2 - \frac{1}{\rho_l} \sigma k(1 + \tilde{\rho})]^{1/2}$$

Numerical evaluation of the second term in Eqn (56) using asymptotic expansion for the modified Bessel's function and its derivative for a typical case showed that it was negligibly small compared to the first term. The unstable wave has been given by Eqns (50) and (51). The rest of the computation followed the plane sheet case.

6. DROPLET DIAMETER DISTRIBUTION

The dispersion relations [Eqns (27) and (46)] merely indicate the most dominant wave modes are used to obtain the MMD. In this, it is obvious that other wave modes are also present and hence droplets of other diameters would also be present in the fuel-air cloud. Thus, this part requires a stochastic sub-model. In³, a lognormal distribution for droplet diameter distribution was presented; however the parameters of the distribution could not be directly related to the parameters of other modules of the mathematical model. It is worth noting that the estimation of MMD from the dispersion relation enables to establish a direct relationship among the droplet diameter distribution model, shock model and the extended near-field model presented here.

The MMD is taken as the mean of the lognormal distribution. Its upper and lower limits come from physical considerations. The upper limit (d_f) is taken approximately as the diameter of the droplet which would travel to the maximum extent of the cloud, taken as 25-30 times of the initial canister diameter. The lower limit (d_i) is assumed to be the minimum droplet diameter below which the liquid droplets become unstable (i.e. evaporate immediately). The lognormal distribution is given by

$$f(x) = \frac{1}{d\sigma\sqrt{2\pi}} \exp\left(-\frac{(x - \mu)^2}{2\sigma^2}\right) \tag{57}$$

where, $\mu = \ln D_{30}$, $\sigma = (\ln d_f - \ln d_i)/6$, $x = \ln d$, d is the droplet diameter.

7. RESULTS & DISCUSSION

Following Gardner's model, an FAE device is considered with the following data for the liquid fuel: Density of the liquid, $\rho_l = 899 \text{ kg/m}^3$, surface tension, $\sigma = 2.42 \times 10^{-2} \text{ N/m}$, dynamic viscosity, $\mu = 3.1 \times 10^{-3} \text{ kg/m-s}$, air density, $\rho_g = 1.2 \text{ kg/m}^3$. The particle velocity in liquid fuel is taken from the shock model, a typical value for U_0 is 140 m/s. Since the sheet thickness $2a$ is not constant in the present case, it varied over a range 1 mm to 10 mm .

Figure 1 shows the disturbance growth factor (ω_r) against the wave number (k) for both the viscous and inviscid cases. The inviscid solution follows from Eqn (53), whereas for the viscous solution, Eqn (52) was numerically solved. The inviscid solution gives $(k_{\max})_{\text{invis}} = 6.4707 \times 10^5$, whereas the viscous solution yields $(k_{\max})_{\text{visc}} = 5.70 \times 10^5$.

Table 1 shows the inviscid and viscous MMD of the droplets for both Rayleigh and atomisation mode of disintegration for various values of the sheet thickness. It is observed that the MMD from the viscous cases result are nearly 8 per cent larger than the corresponding inviscid cases. Further, it is observed that the MMDs of the droplets given by Rayleigh mode are many times larger than those given by the atomisation mode. It may be noted that droplets with diameters larger than 100 μm cannot stay floating in air and will fall down under the

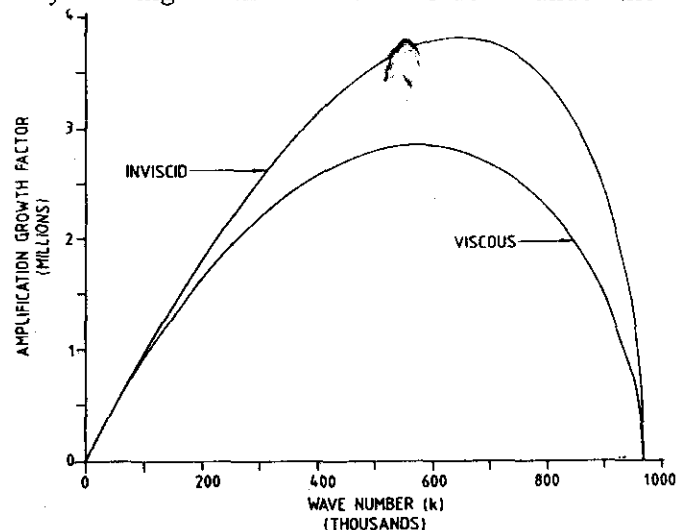
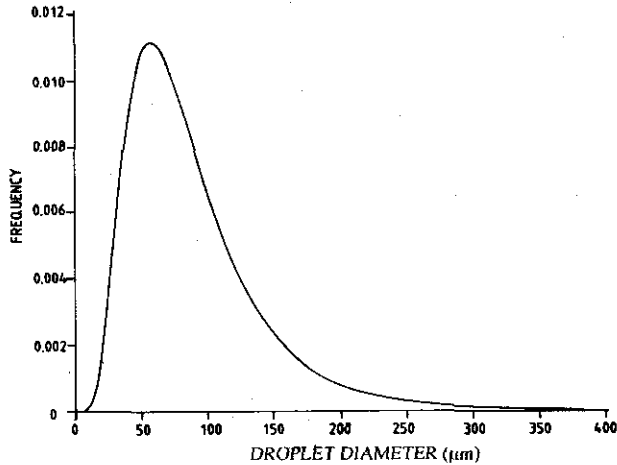


Figure 1. Amplification growth factor ω_r versus wave number k .

Table 1. Inviscid and viscous mean-mass diameters for both Rayleigh and atomisation modes

Sheet thickness (mm)	$(D_{Ray})_{inv}$ (μm)	$(D_{Ray})_{vis}$ (μm)	$(D_{Atom})_{inv}$ (μm)	$(D_{Atom})_{vis}$ (μm)
1	148.59071	158.31688	35.57430	38.71243
2	210.13899	223.89388	44.82081	48.77460
3	257.36664	274.21286	51.30701	55.83298
4	297.18143	316.63376	56.47068	61.45215
5	332.25894	354.00726	60.83120	66.19732
6	363.97140	387.79556	64.64279	70.34515
7	393.13406	418.86706	68.05119	74.05421
8	420.27801	447.78775	71.14860	77.42486
9	445.77210	474.95062	73.99752	80.52509
10	469.88507	500.64191	76.64250	83.40340

effect of gravity¹³. Thus, even the formation of clouds would not be possible for such large droplets. On the other hand, the MMDs of droplets given by the atomisation mode are more realistic; the droplets with these diameters would result in a stable aerosol cloud which may be subsequently detonated by a secondary mechanism.

**Figure 2. Distribution of droplet diameters**

In Fig. 2, the lognormal distribution of the droplet diameters for a typical MMD (corresponding to a sheet thickness of 6 mm in atomisation mode) is shown, with the MMD as the mean of the distribution.

REFERENCES

- Kennedy, D.R. Warheads: A historical perspective. *In* Tactical missile warheads, edited by Joseph Carlene. Progress in Astronautics and Aeronautics, Vol. 155, AIAA Inc., USA, 1993.
- Gardner, D. R. Near-field dispersal modelling for liquid fuel-air explosives. Sandia Report No. SAND-90-0686, 1990.
- Singh, V.P. & Singh, S.K. Fuel-air explosives: A review of mathematical models. Proceedings of the Symposium on Systems Analysis for Defence, CASSA, Bangalore, 25-26 September 1997. pp. 247- 54.
- Sihota, B.S. Fuel-air explosive – high performance force multiplier armament system for soft targets. Paper presented in National Workshop on Force Multiplier Armament System, 1996.
- Glass, M.W. Far-field dispersal modelling for fuel-air explosive devices. Sandia Report No. SAND-90-0528, 1990.
- Dombrowski, N. & Johns, W.R. The aerodynamic instability and disintegration of viscous liquid sheets. *Chemical Engg. Sc.*, 1963, **18**, 203-14.
- Li, X. & Tankin, R.S. On the temporal instability of a two-dimensional viscous liquid sheet, *J. Fluid Mech.*, 1991, **226**, 425- 43.
- Mitra, S.K. & Li, X. Initial distribution of droplet sizes in sprays. Proceedings of the 2nd International HEMCE, IIT Madras, Chennai, December 8-10, 1990, pp. 535-41.
- Lin, S.P. & Kang, D. Atomisation of a liquid jet. *Physics of Fluids*, 1987, **30** (7), 2000-06.
- Drazin, P.G. & Reid, W.H. Hydrodynamic stability. Cambridge University Press, 1981.
- Milne-Thomson, L.M. Theoretical hydrodynamics, Ed. 4. Macmillan, London, 1962.
- Strutt, J. W. (Lord Rayleigh) The theory of sound, Vol II. Dover Publications, 1945.
- Reist, P.C. Aerosol science and technology, Ed. 2. McGraw-Hill Inc., 1993.

Capillary Wave at the Interface of Liquid and Gas

The equation for the wave propagation at the liquid-gas interface in the absence of gravity is¹¹:

$$k\rho_l(U_0 - c)^2 \coth(ka) + k\rho_g c^2 \coth(ka') = \sigma k^2 \quad (\text{A1})$$

where c is the wave propagation velocity, a , a' are the thicknesses of the liquid and gas layers, respectively. In the present case, $a' \rightarrow \infty$ (as the air extends up to infinite extent), hence $\coth(ka') \rightarrow 1$, also as noted earlier, the wave number k has a large value in the present case, hence $\coth(ka) \rightarrow 1$ and Eqn (A1) reduces to

$$(U_0 - c)^2 + \tilde{\rho}c^2 = \frac{\sigma k}{\rho_l} \quad (\text{A2})$$

which gives

$$c = (1 + \tilde{\rho})^{-1} \left[U_0 \pm \left\{ U_0^2 - (1 + \tilde{\rho}) \left(U_0^2 - \frac{\sigma k}{\rho_l} \right) \right\}^{1/2} \right] \quad (\text{A3})$$

If $\tilde{\rho}U_0^2 > \sigma k(1 + \tilde{\rho})/\rho_l$, then the wave velocity c becomes imaginary. Let

$$m^2 = \tilde{\rho}U_0^2 - \frac{\sigma k(1 + \tilde{\rho})}{\rho_l}$$

then from Eqn (A3), one gets:

$$c = (1 + \tilde{\rho})^{-1} (U_0 \pm im) \quad (\text{A4})$$

Since $c = -\omega_i/k$, one can obtain from Eqn (A4)

$$\omega_i = -\frac{kU_0}{1 + \tilde{\rho}} \pm \frac{ikm}{1 + \tilde{\rho}} \quad (\text{A5})$$

Since $\omega = \omega_r + i\omega_i$, hence the real part of ω is:

$$\text{Re } \omega = \omega_r \pm \frac{km}{1 + \tilde{\rho}} \quad (\text{A6})$$

It may be noted that instability occurs (i.e. $\omega_r > 0$) only when

$$\tilde{\rho}U_0^2 > (1 + \tilde{\rho}) \frac{\sigma k}{\rho_l} \quad (\text{A7})$$

and $\omega_i \equiv 0$ when $\tilde{\rho}U_0^2 \leq (1 + \tilde{\rho})\sigma k/\rho_l$.